Acta Diabetologica (2019) 56:457–472
https://doi.org/10.1007/s00592-018-1273-1

ORIGINAL ARTICLE

RAGE/galectin-3 yields intraplaque calcification transformation via sortilin

Zhen Sun[1] · Zhongqun Wang[1] · Lihua Li[2] · Jinchuan Yan[1] · Chen Shao[1] · Zhengyang Bao[1] · Lele Jing[1] · Qiwen Pang[1] · Yue Geng[1] · Lili Zhang[1]

Received: 18 October 2018 / Accepted: 10 December 2018 / Published online: 2 January 2019

Abstract

Aims Macrocalcification and microcalcification present different clinical risks, but the regulatory of their formation was unclear. Therefore, this study explored the underlying mechanisms of macrocalcification and microcalcification in diabetes mellitus.

Methods Anterior tibial arteries of amputated diabetic feet were collected. According to the calcium content, patients were divided into less-calcification group and more-calcification group. And calcification morphology in plaques was observed. For further study, an in vivo mouse diabetic atherosclerosis model and an in vitro primary mouse aortic smooth muscle cell model were established. After the receptors for AGEs (RAGE) or galectin-3 were silenced, calcified nodule sizes and sortilin expression were determined. Scanning electron microscopy (SEM) was performed to detect the aggregation of matrix vesicles with the inhibition or promotion of sortilin.

Results Both macro- and microcalcification were found in human anterior tibial artery plaques. Macrocalcification formed after the silencing of RAGE, and microcalcification formed after the silencing of galectin-3. In the process of RAGE- or galcetin-3-induced calcification, sortilin played an important role downstream. SEM showed that sortilin promoted the aggregation of MVs in the early stage of calcification and formed larger calcified nodules.

Conclusion RAGE downregulated sortilin and then transmitted microcalcification signals, whereas galectin-3 upregulated sortilin, which accelerated the aggregation of MVs in the early stage of calcification and mediated the formation of macrocalcifications, These data illustrate the progression of two calcification types and suggest sortilin as a potential target for early intervention of calcification and as an effective biomarker for the assessment of long-term clinical risk and prognosis.

Keywords Vascular calcification · Matrix vesicle · RAGE · Galectin-3 · Sortilin

Abbreviations

VSMCs	Vascular smooth muscle cells
CML	*Nε*-carboxymethyl-lysine
AGEs	Advanced glycation end products
RAGE	Receptor for advanced glycation end products
GWAS	Genome-wide association study
SPF	Specific pathogen free
STZ	Streptozotocin
AAV	Adeno-associated viral
OM	Osteogenic medium
LV	Lentivirus vector
oxLDL	Oxidized low-density lipoprotein
CoIP	Coimmunoprecipitation
SEM	Scanning electron microscopy
NTA	Nanoparticle tracking analysis
MVs	Matrix vesicles
HFD	High-fat diet
RUNX2	Runt-related transcription factor 2
PBS	Phosphate-buffered saline
TNAP	Tissue nonspecific alkaline phosphatase
EVs	Extracellular vesicles
CCK-8	Cell counting kit-8
MOI	Multiplicity of infection

Managed By Massimo Porta.

Zhen Sun and Zhongqun Wang contributed equally to this work.

Electronic supplementary material The online version of this article (https://doi.org/10.1007/s00592-018-1273-1) contains supplementary material, which is available to authorized users.

✉ Zhongqun Wang
wangtsmc@aliyun.com

Extended author information available on the last page of the article

Introduction

Diabetes mellitus is a serious threat to human health. Approximately, 5.2 million people die of diabetes each year, and it is estimated that 642 million people will suffer from diabetes by 2040 [1]. Diabetes is defined by the impairment of glycometabolism and can lead to other systemic metabolic disorders, such as abnormal lipid metabolism and bone metabolic dysfunction. These metabolic imbalances can cause irreversible harm to patients [2]. Studies have found that 78% of diabetics have varying degrees of vascular calcification, which can further increase the risk of heart or kidney disease and greatly increase mortality [3]. Therefore, it is essential to explore the potential mechanisms of diabetic vascular calcification.

According to morphology, vascular calcifications can be classified into microcalcifications and macrocalcifications. Microcalcifications includes undetectable microcalcification (< 30 μm) and spotty calcification (30–100 μm). Macrocalcifications are categorized into early macrocalcifications (100–200 μm) and large calcifications (≥ 200 μm) [4, 5]. Clinical risks are also different between the two vascular calcification patterns: microcalcifications usually form vulnerable plaques, during which acute cardiovascular events tend to occur, while macrocalcifications have increased plaque stability [6]. Long-term macrocalcifications can lead to a significant decrease in vascular compliance and subsequent heart failure [7]. Fomer reports suggest that osteogenic trans-differentiated vascular smooth muscle cells (VSMCs) can increase calcified lesion, and calcification inhibitors can prevent this process [8, 9]. However, the mechanisms underlying the formation of macro- or microcalcification still remain unclear.

Our previous study found that *N*ε-carboxymethyl-lysine (CML), the main component of advanced glycation end products (AGEs), has a pro-calcification effect [10]. CML and the receptor for advanced glycation end products (RAGE) produce CML/RAGE calcification cascade signals that mostly contribute to the formation of microcalcifications rather than macrocalcifications [11]. During the process of mineralization, RAGE plays a role in delivering osteoclast signals [12], while galectin-3, another major receptor of AGEs, functions in regulating osteogenesis [13]. Menini et al. [9] found that RAGE and galectin-3 played opposite roles in the formation of microcalcification and macrocalcification. This is based on cellular levels, so more in vivo experiments are needed to confirm this conclusion. And, the mechanism of RAGE and galectin-3 in mediating the formation and morphology of calcified nodules is unclear.

Sortilin is a key member of the Vps10p domain receptor family that is involved in various cell functions [14, 15]. A genome-wide association study (GWAS) revealed that the *SORT1* gene is closely associated with many human diseases, such as myocardial infarction and atherosclerosis [16]. Recent studies have also found that sortilin affects in vivo metabolism and is a key player in glucose and lipid metabolism disorders [17, 18]. These disorders act as initiating factors for atherosclerosis and vascular calcification. So, we speculated that sortilin may be a key molecular switch in the regulation of calcification types by RAGE/galectin-3.

In this study, we collected the anterior tibial arteries of diabetic foot amputations and used an in vivo and an in vitro vascular calcification model to elucidate the regulatory mechanisms of macrocalcification or microcalcification formation. This may provide new perspectives for the prevention, treatment and prognosis of diabetic vascular calcification.

Methods

Patients

All 30 patients gave consent and received amputation surgery in the Department of Orthopedics, Affiliated Hospital of Jiangsu University (Zhenjiang, China). This study conforms to the principles outlined in the Declaration of Helsinki and was approved by the Ethical Committee of the Affiliated Hospital of Jiangsu University. These type 2 diabetic patients had no history of severe trauma or tumors and underwent amputation because of diabetic foot from March 2016 to December 2017. Prior to amputation surgery, medical history assessments including age, sex, height, weight, fasting blood glucose, cholesterol, and triglycerides were performed. Patients with a history of stomach ulcers, gastrectomy, taking hormones, or taking metformin were excluded. For each artery, the calcium content of the three most severe lesions was measured, and the mean calcium content was taken as the basis for grouping. Then, according to the determination of calcium content, the patients were divided into less calcification group (< 5 μmol/mg) and more calcification group (≥ 5 μmol/mg).

Animals

4-week-old ApoE$^{-/-}$ mice on a C57BL/6J background were purchased from Vital River Laboratories (Distributor of Jackson Laboratory, Beijing, China). All animals lived in a specific pathogen-free (SPF) environment. The mice were given an intraperitoneal injection of streptozotocin (STZ; 40 mg/kg/day) for 5 days. 2 weeks after the initial STZ injection, mice with blood glucose of > 300 mg/dL were included in this study. Subsequently, 10^{12} DNAse-resistant particles of adeno-associated

viral (AAV) vectors consisting of AAV-shscramble (as a control group), AAV-shRAGE, or AAV-shgalectin-3 (Han Heng Biological Technology Co., Ltd. Shanghai China) solution was injected into mice via the tail vein. 3 weeks after AAV injection, the high-fat diet (HFD) was introduced. CML (10 mg/kg/day) diluted in normal saline or recombinant sortilin protein (0.1 mg/kg/day) or sortilin-neutralizing antibody (0.1 mg/kg/day) were injected into tail veins for 6 weeks. Blood glucose levels were assessed by tail blood sampling at 3, 6, 9, 12, and 15 weeks after CML injection. Mice were euthanized with 90 mg/kg sodium pentobarbital. The thoracic aorta and aortic arch were separated under a dissecting microscope. After paraffin embedding, consecutive sections were taken, and calcified areas were selected for follow-up experiments (Supplementary Fig. S1). All animal experiments were approved by the Animal Health and Utilization Committee of the Affiliated Hospital of Jiangsu University, and carried out in accordance with the guidelines from Directive 2010/63/EU. The animal groups were as follows: NC group (ordinary feed diet only), HFD group (high-fat diet only), CML group (HFD + CML), AAV-shscramble group (HFD + AAV-shscramble), AAV-shRAGE group (HFD + AAV-shRAGE), AAV-shgalectin-3 group (HFD + AAV-shgalectin-3), double intervention group (HFD + AAV-shRAGE + AAV-shgalectin-3), AAV-shRAGE + sortilin group, AAV-shRAGE + anti-sortilin group, AAV-shgalectin-3 + sortilin group, and AAV-shgalcetin-3 + anti-sortilin group.

Cell culture and diabetic vascular calcification model

The mice were sacrificed by cervical dislocation and placed in 75% ethanol for 5 min. After full exposure of the chest cavity, the thoracic aorta was removed and the blood vessel was longitudinally dissected. Then, the external layer was cleaned, the internal layer was scraped with an ophthalmic file and the middle layer was peeled off completely. The tunica media was cut into 1–2 mm tissue pieces and placed evenly on the bottom of a 25 cm flask. 5 mL of DMEM/F12 medium containing 20% fetal bovine serum was added and incubated at 37 °C in a 5% CO_2 incubator. The cells were passaged when grown to 70% confluence. Osteogenic medium (OM, 2.5 mM β-glycerophosphate and 50 μg/mL ascorbic acid) was added to induce cell calcification. The mock group, LV-shRAGE group, LV-shgalectin-3 group, double intervention group (treated with LV-shRAGE and LV-shgalectin-3), LV-shRAGE + scramble group, LV-shRAGE + siRNA group, LV-shgalectin-3 + scramble group and LV-shgalectin-3 + siRNA group were pretreated with lentivirus vector or siRNA before adding OM. To simulate the environment of diabetic patients, 50 μg/mL oxidized low-density lipoprotein (oxLDL) and CML were also added during calcification induction. Different CML concentrations of 0, 5, 10, and 20 μmol/L and three different time points of 0, 7, and 14 days were used to determine the optimal conditions for CML.

Cell viability measurement

Cell viability assay was conducted with the Cell Counting Kit-8 (CCK-8, Beyotime Institute of biotechnology, Haimen, China). Cells were seeded into 96-well culture plates at 1×10^5 cells/well. And, after lentivirus transduction or further siRNA transfection, the cell viability was determined by CCK-8 according to manufacturer's instructions.

Calcium content quantification

Quantification of calcium content was previously described [2]. In brief, the dehydrated, dried aorta (approximately 10 mg) or cells were decalcified with 0.6 N HCl for 24 h at room temperature. Free calcium was then determined using the o-cresolphthalein complex ketone method (QuantiChromTM Calcium Assay Kit, BioAssay Systems, USA). The sample was then washed with phosphate-buffered saline (PBS) and dissolved in 0.1 mol/L NaOH and 0.1% sodium dodecyl sulfate (SDS) for protein concentration analysis. The protein content was measured with BCA Protein Assay Kit (Nanjing Jiancheng Bioengineering Institute, China). Experimental steps followed the manufacturer's instructions. Finally, calcification deposition was normalized to the amount of total protein.

Serological tests

Fasting patient or mouse blood serum was collected, and serum was separated and stored at − 80 °C. All samples were measured on the same day. The levels of human CML and mouse sortilin were measured using an ELISA kit (Nanjing Jiancheng Bioengineering Institute, China). All steps followed the manufacturer's instructions.

Immunofluorescence

Cells or tissues were fixed with 5% formaldehyde for 30 min. After washing with PBS, 0.2% Triton X-100 was added for 10 min to initiate permeabilization. The samples were then incubated with 1% bovine serum albumin for 1 h at 37 °C. Primary antibody was diluted and incubated for 16 h. After washing the sample in PBS, secondary fluorescent antibody was added and incubated for 1 h in the dark. Images were taken under an inverted microscope (IX51, Olympus Corporation, Tokyo, Japan). The antibodies used were: anti-RAGE (ab216329, Abcam, 1:100, Cambridge, UK); anti-galectin-3 (ab76245, Abcam, 1:1000); anti-sortilin (ab16640, Abcam, 1 μg/mL); anti-α-SMA(F3777, Sigma–Aldrich, 1:500, St. Louis, MO, USA).

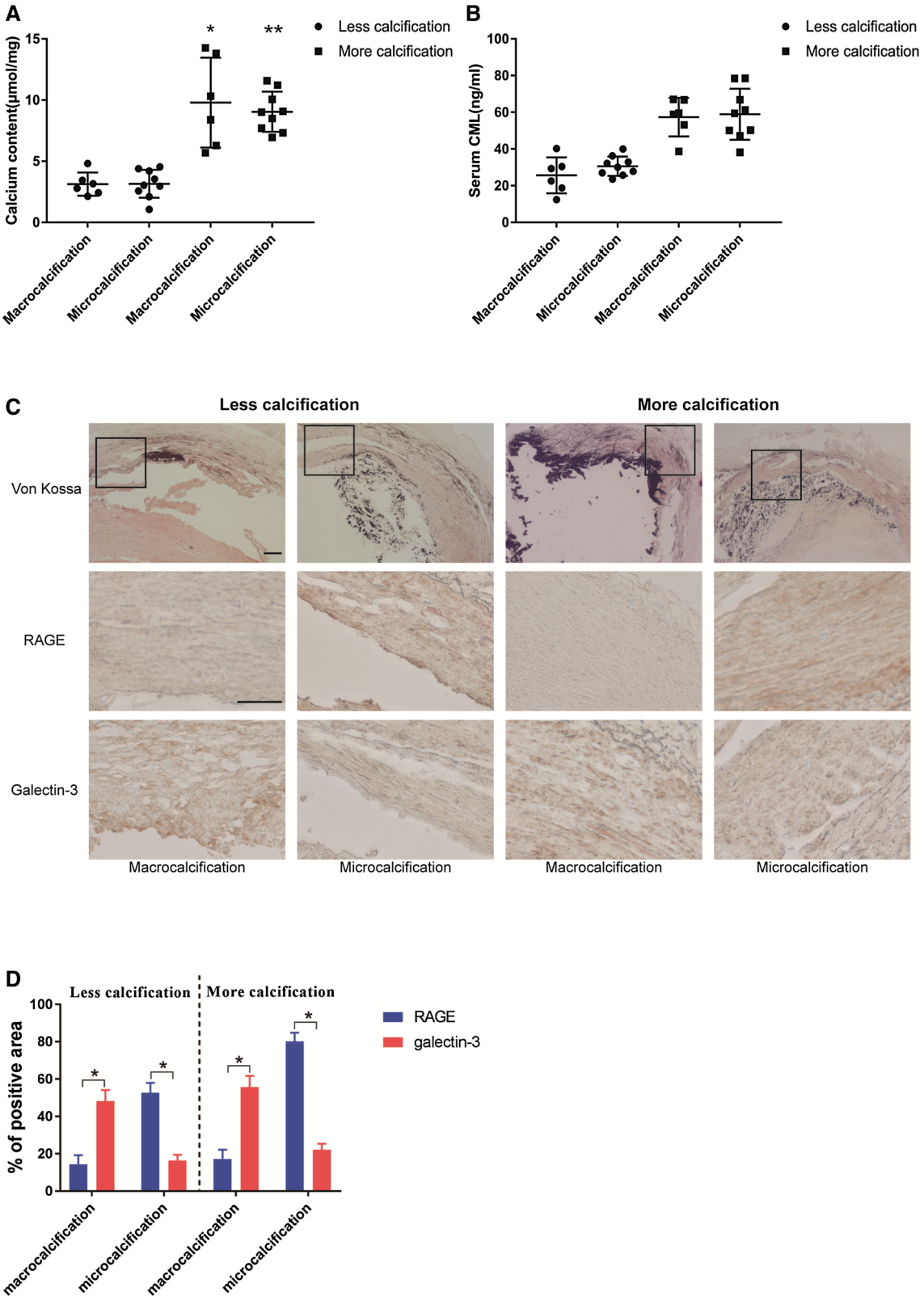
A
Calcium content(μmol/mg)
15
10
5
0
*
**
Less calcification
More calcification
Macrocalcification
Microcalcification
Macrocalcification
Microcalcification
B
Serum CML(ng/ml)
100
80
60
40
20
0
Less calcification
More calcification
Macrocalcification
Microcalcification
Macrocalcification
Microcalcification
C
Less calcification
More calcification
Von Kossa
RAGE
Galectin-3
Macrocalcification
Microcalcification
Macrocalcification
Microcalcification
D
Less calcification
More calcification
% of positive area
100
80
60
40
20
0
*
*
*
*
RAGE
galectin-3
macrocalcification
microcalcification
macrocalcification
microcalcification

◂**Fig. 1** RAGE and galectin-3 expression in arteries from amputated diabetic foot samples were different in macro- and microcalcifications. **a–d** According to the calcified nodule size of plaques, the less calcification group and more calcification group were further divided into macrocalcification and microcalcification conditions. **a** Calcium content was tested. $*p<0.05$ compared with macrocalcification of the less calcification group; $**p<0.05$ compared with microcalcification of the less calcification group. **b** Serum CML of patients with macrocalcifications or microcalcifications was detected by enzyme-linked immunosorbent assay (ELISA). **c** First row: von Kossa staining shows the two calcification patterns of the less and more calcification groups. Black: calcium deposition. Scale bar 100 μm. Second and third row: immunohistochemistry shows the expression of RAGE and galectin-3. Bar represents 50 μm. Representative images are shown. **d** Percentage of positive immunohistochemical staining area. After immunostaining with RAGE and galectin-3 antibodies, four images of vascular smooth muscle from different fields were randomly selected. The proportion of the positive area to the total smooth muscle area was calculated by ImageJ. $*p<0.05$, in two-sample unpaired *t* test

Immunohistochemistry

Paraffin sections were deparaffinized and rehydrated and boiled in citrate buffer for 20 min for antigen retrieval. Sections were blocked with 5% goat serum for 1 h at room temperature. Human samples were incubated with anti-RAGE (ab216329, Abcam, 1:4000) and anti-galectin-3 (ab76245, Abcam, 1:250) at 4 °C overnight. The rest of the steps were performed using the SP Rabbit & Mouse HRP Kit (Kangwei Century Biotechnology Co., Ltd. China). Finally, samples were photographed under a microscope (Olympus).

Von Kossa staining and Alizarin red staining

For von Kossa staining, cells or tissues were incubated with 5% silver nitrate under sunlight until they turned black. 5% sodium thiosulfate solution was then added for 5 min to remove unreacted silver. After washing three times with deionized water, neutral fuchsin was used to counterstain for 3 min followed by washing for observation under a microscope (Olympus). For Alizarin red staining, samples were washed twice with phosphate-buffered saline, fixed in 4% paraformaldehyde at 4 °C for 5 min, and stained with 2% Alizarin red (pH 4.2) for 5 min at room temperature. Samples were then rinsed with deionized water and observed. Alizarin red-stained samples were extracted with 10% cetylpyridinium chloride for 10 min. The OD value was measured at 570 nm with a spectrophotometer.

Western blot and semi-quantitative RT-PCR analysis

For immunoblots, cells were lysed with RIPA lysis buffer for total protein. Samples were separated by SDS–PAGE and transferred to a nitrocellulose membrane. After the blocking with 5% nonfat milk, membranes were then incubated with sortilin (ab16640, Abcam, 1 μg/mL), RUNX2 (YT5356, ImmunoWay, 1:1000), β-actin (#4967, Cell Signaling Technology, 1:1000, Danvers, MA, USA), CML (ab125145, Abcam, 1:2000), RAGE (ab216329, Abcam, 1:1000) or galectin-3 (ab76245, Abcam, 1:5000) antibodies overnight at 4 °C. Then, the membranes were washed with TBST, and diluted secondary antibody (1:5000) was added and incubated at 37 °C for 1.5 h. After enhancement with the ECL detection kit (Bio-Rad, Hercules, CA, USA), analysis was performed with a gel imaging system (Amersham Imager 600). For RT-PCR, total RNA was isolated using Trizol reagent (Invitrogen, Carlsbad, CA, USA) and reverse transcribed into cDNA. Real-time PCR was performed using primers for mouse RAGE, galectin-3 and β-actin (Sangon Biotech, China). Primer sequences are detailed in Supplementary Table S1. The RT-PCR detection conditions were: 94 °C for 1 min followed by 33 cycles at 94 °C for 30 s, 63 °C for 30 s, 72 °C for 1 min, and a final extension at 72 °C for 7 min.

Lentivirus transduction and siRNA transfection

For lentiviral vector infections, cells were seeded in 6-well plates at a density of 1×10^5. The virus-containing stock solution (Han Heng Biological Technology Co., Ltd. Shanghai China) was mixed with a complete medium containing 10 μg/mL polybrene in a 1:1 ratio and added to the cells at a multiplicity of infection (MOI) of 30. After 16 h of infection, the medium was changed and cells were selected with 2 μg/mL puromycin for 3 days. For siRNA transfection, cells were co-incubated with 50 nM siRNA in serum-free medium for 6 h. Then, the medium was changed to serum-containing medium. Transfection efficiency was enhanced using Lipofectamine 2000 (1:25, Invitrogen).

Coimmunoprecipitation (CoIP)

Tissue proteins were extracted by cutting the tissues into 2 mm × 2 mm pieces. 100–200 CoIP buffer was added per 20 mg tissue (50 mM Tris/HCl pH 8.0, 150 mM NaCl, 5 mM EDTA, 0.5% NP-40, 1 mM phenylmethylsulfonyl fluoride, 2 μg/mL aprotinin, 2 μg/mL leupeptin and 2 μg/mL pepstatin) for 30 min on ice. Samples were homogenized with a glass homogenizer until fully lysed then centrifuged at $12{,}000\times g$ for 5 min, and the supernatant was taken for subsequent experiments. Protein A/G agarose (YEASEN Biotechnology Co., Ltd. Shanghai China) was used to eliminate nonspecific protein binding. Primary antibody was added and samples were slowly shaken overnight at 4 °C. Samples were then centrifuged $14{,}000\times g$ for 5 min to collect the precipitate, which was analyzed by Western blot. The antibodies used were: anti-RAGE (ab216329, Abcam, 1:30) and anti-CML (ab125145, Abcam, 1:50).

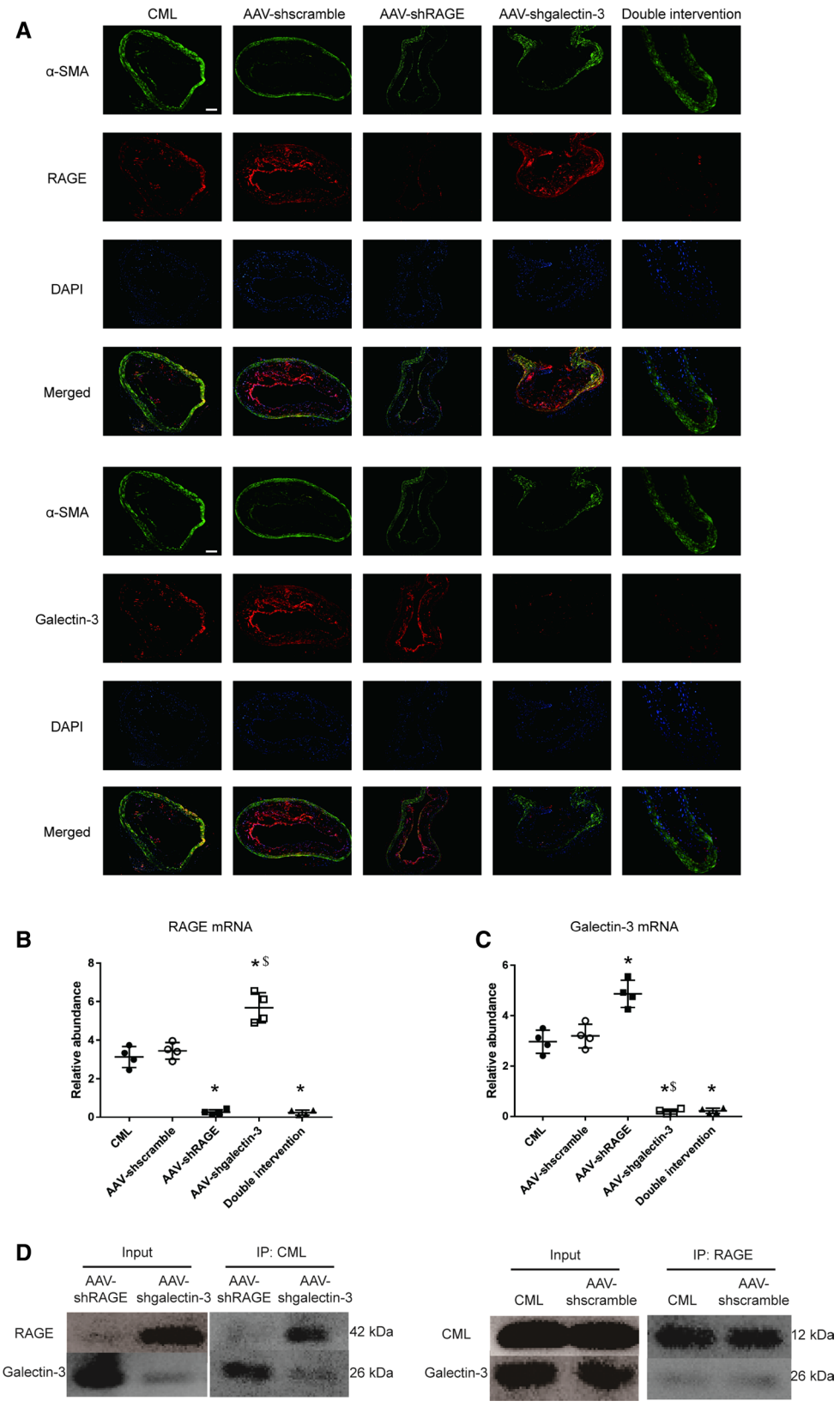

Fig. 2 RAGE and galectin-3 expression in the diabetic atherosclerosis mouse model changed after AAV injection. **a** Representative images of RAGE and galectin-3 immunostaining are shown ($n=5$ mice in each group); green: α-SMA, red: sortilin, blue: nucleus, orange: co-localization of α-SMA and RAGE/galectin-3. Scale bar 100 μm. **b, c** RAGE and galectin-3 mRNA levels in mouse aortas were tested at the 3rd week after AAV injection ($n=4$ independent experiments). $^{*}p<0.05$ compared with AAV-shscramble group. $^{\$}p<0.05$ compared with AAV-RAGE group. **d, e** CoIP shows the interaction between CML, RAGE and galectin-3. **d** CML interacted with RAGE or galectin-3. **e** RAGE had no interaction with galectin-3. (Color figure online)

Scanning electron microscopy (SEM)

Before obtaining micrographs of samples, a critical point dryer (PVT-3, Tousimis Semidri, Rockville, MD, USA) was used to completely evaporate water from the samples. Then, the samples were coated with a 10 nm gold layer under a vacuum and inspected with SEM (SU8000 and S4800, Hitachi, Tokyo, Japan).

Matrix vesicles isolation and nanoparticle tracking analysis (NTA)

During the induction of calcification, OM was gradually replaced by media containing the same components but with a low concentration of serum (0.1%) to reduce its interference with vesicles. As previously described [19], ultra-centrifugation (L-70, Beckmann Coulter, USA) was used for matrix vesicles (MVs) isolation. In brief, media was centrifuged at 20,000 × *g* for 30 min at 4 °C to remove cellular contaminants. Then, the supernatant was further centrifuged at 100,000 × *g* for 60 min at 4 °C. After removing the supernatant, MVs were resuspended in fresh calcifying medium and divided into three parts for NTA. The three portions were incubated at 37 °C for 1, 4, or 7 days and detected with NTA to determine the size distribution of MVs aggregates. All experiments were performed with an NTA machine (LM10, Malvern Instruments Ltd, UK). Samples were diluted and at least three NTA videos were taken for 1 min each with background level 10, camera level 12 and shutter speed 1/30 s.

Statistical analysis

Data are expressed as means ± SD. SPSS 11.0 software was used for data analysis. Student's *t* test or one-way analysis of variance was used for comparison between the two groups. One-way ANOVA was used for comparisons among three groups. Pearson correlation analysis was used for correlation analysis. $p < 0.05$ was considered statistically significant.

Results

RAGE and galectin-3 expression are different in macro- and microcalcifications

Baseline information is shown in Table S2. There were no significant differences in age, BMI, fasting blood glucose, total cholesterol, or triglycerides between the less and more calcification group except for the diabetes duration and serum CML. However, there was no significant difference in the calcium content (Fig. 1a) or the serum CML (Fig. 1b) between the macrocalcifications and microcalcifications within each calcification group. Von Kossa staining shown in the first row of Fig. 1c indicated that macro- and microcalcified nodules both exist in the more and less calcification groups. So, it can be speculated that calcification type is not associated with calcium content and CML level. Furthermore, immunohistochemistry (Fig. 1c second and third row; Fig. 1d) shows that RAGE expression was significantly lower than galectin-3 in macrocalcified vascular smooth muscle, while in microcalcified conditions RAGE level was significantly higher than galectin-3. This result was consistent with the finding of Menini et al. [9]. Therefore, RAGE and galectin-3 may play different roles in the mediation of diabetic vascular calcification.

Silencing either RAGE or galectin-3, the other increased

To verify our hypothesis, an in vivo model was constructed. Apolipoprotein E knockout ($ApoE^{-/-}$) mice are commonly used as models of atherosclerosis. After the introduction of HFD, the body weight line began to rise (Supplementary Fig. S2A) and reached their highest level at about the 9th week. Mice in CML group and CML combined with AAV treatment group (AAV-shscramble group, AAV-shRAGE group, AAV-shgalectin-3 group, and double intervention group) all began to lose weight after the 9th week, indicating that the injection of AAV did not influence the change of body weights. After the injection of CML, the blood glucose of mice continued to increase (Supplementary Fig. S2b). AAV injection did not affect the change of blood glucose too. In the HFD group, the blood glucose levels rose steadily after the 3rd week, possibly due to the dysfunctional lipid metabolism. RAGE or galectin-3 immunofluorescence (Fig. 2a) and its quantification (Supplementary Fig. S3) show that RAGE and galectin-3 expression did not change significantly after the injection of AAV-shscramble. AAV-shRAGE significantly downregulated the expression of RAGE, while galectin-3 increased obviously. Additionally, after AAV-shgalectin-3 injection, galectin-3 significantly decreased, while RAGE was markedly upregulated. The changes in RAGE and galectin-3 mRNA (Fig. 2b, c) were consistent with protein expression. Since the injection of AAV came before atherosclerosis, changes in RAGE and galectin-3 expression in plaques were not completely consistent with those in vascular smooth muscle. So, we detected RAGE and galectin-3 mRNA at the 3rd week after AAV injection, at a time when vascular plaques had not formed. We also found that CML could interact with both RAGE and galectin-3 (Fig. 2d), whereas RAGE and galectin-3 did not interact with each other (Fig. 2e).

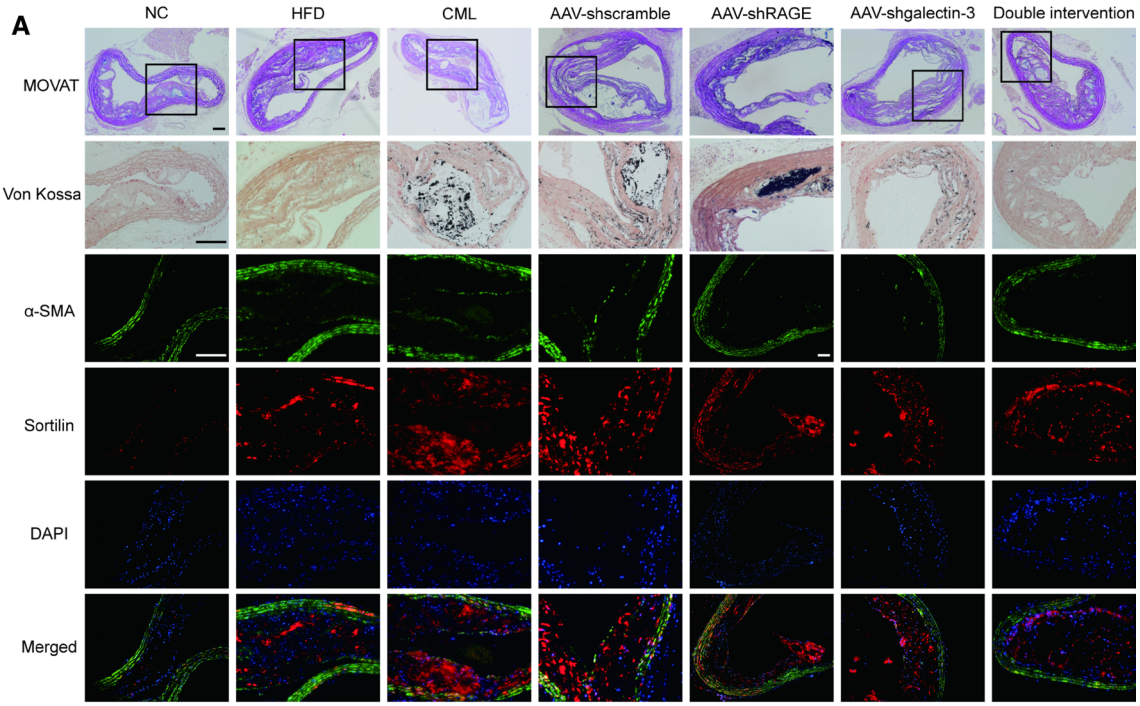
A
NC
HFD
CML
AAV-shscramble
AAV-shRAGE
AAV-shgalectin-3
Double intervention
MOVAT
Von Kossa
α-SMA
Sortilin
DAPI
Merged

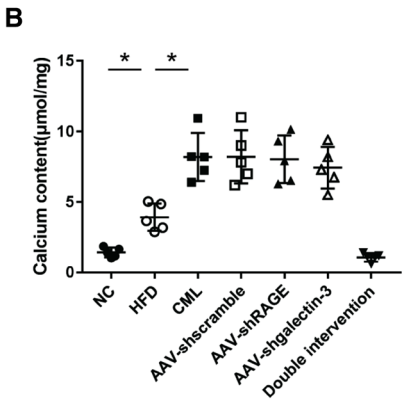
B
Calcium content(μmol/mg)
15
10
5
0
*
*
NC
HFD
CML
AAV-shscramble
AAV-shRAGE
AAV-shgalectin-3
Double intervention

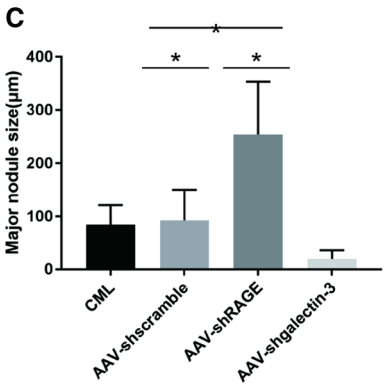
C
Major nodule size(μm)
400
300
200
100
0
*
*
*
CML
AAV-shscramble
AAV-shRAGE
AAV-shgalectin-3

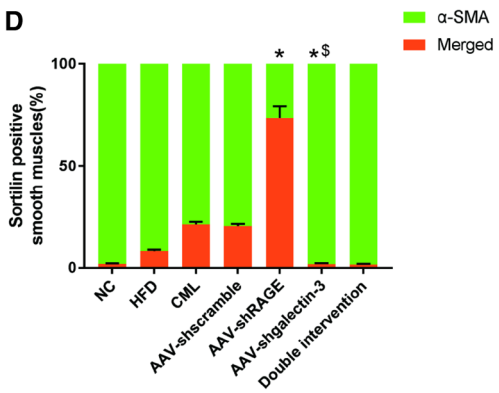
D
α-SMA
Merged
Sortilin positive smooth muscles(%)
100
50
0
*
*$
NC
HFD
CML
AAV-shscramble
AAV-shRAGE
AAV-shgalectin-3
Double intervention

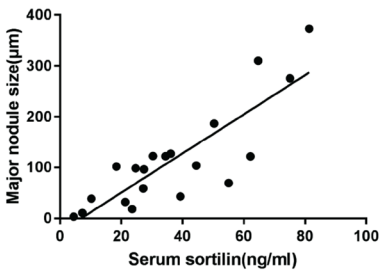
Major nodule size(μm)
400
300
200
100
0
0
20
40
60
80
100
Serum sortilin(ng/ml)

◂**Fig. 3** RAGE/galectin-3 regulated the calcification progression and type in the diabetic atherosclerosis mouse model. **a–d** RAGE/galectin-3 influenced sortilin expression of vascular smooth muscles and calcium nodule size. **a** 1st row, Movat pentachrome staining shows the gross morphology of vascular smooth muscles. Boxes show the regions of immunofluorescence images below. **a** 2nd row, von Kossa staining shows the largest calcium nodules of mouse aortas in continuous slices ($n=3$ mice). **a** Line 3–6, the location of vascular smooth muscles and sortilin-positive area is shown by immunostaining ($n=5$ mice in each group). green: α-SMA, red: sortilin, blue: nucleus, orange: co-localization of α-SMA and sortilin. Scale bar 100 μm. **b** Calcium content of mouse aortas was measured ($n=5$ independent experiments). **c** Mean diameters of aortic calcium nodules in mice $^{*}p<0.05$; $^{**}p<0.001$ in two-sample unpaired t test. **d** Percentage of sortilin-positive smooth muscle area. After immunofluorescence staining, images of four different visual fields were randomly chosen. The proportion of the sortilin-positive smooth muscle area (orange area) was calculated with Image J. $^{*}p<0.05$ compared with the AAV-shscramble groups. $^{\$}p<0.05$ compared with the AAV-shRAGE group. **e** Pearson correlation analysis shows the relation between serum sortilin and the maximum diameter of calcification nodules ($r=0.843$, $p<0.05$). (Color figure online)

RAGE and galectin-3-mediated calcification patterns in mouse aorta

Calcium content in mice aortas significantly increased after HFD (Fig. 3b) and increased to 2.09-fold that of the HFD group (8.21 ± 1.71 vs. 3.92 ± 0.97 μmol/mg, $p<0.05$) after CML treatment (CML group). Injection of AAV-shscramble, AAV-shRAGE or AAV-shgalectin-3 had no significant effect on the calcium content. In terms of calcification morphology (Fig. 3a, c), mean diameters of the CML group were at the tipping point of macrocalcifications and microcalcifications (83.75 ± 37.42 μm). AAV-shscramble had no significant influence on calcification morphology. Compared with the AAV-shscramble group, the diameters of calcified nodules were obviously larger in the AAV-shRAGE group (254.58 ± 98.79 vs. 92.16 ± 58.23 μm, $p<0.05$). When AAV-shgalectin-3 was injected, the calcified nodules became significantly smaller and tended to form microcalcifications (20.26 ± 15.82 μm). When both RAGE and galectin-3 were silenced (the double intervention group), the calcium content decreased to the level of the NC group (1.08 ± 0.29 vs.1.43 ± 0.34 μmol/mg, ns), which may be due to the blockage of calcification cascade signaling. Because of the significant decrease of calcium content, the calcium nodule size of the double intervention group was not compared with the AAV-shRAGE group or AAV-shgalectin-3 group. We also measured the expression of sortilin in arteries (Fig. 3a, lines 3–6). Compared with the AAV-shgalectin-3 group, more sortilin-positive smooth muscle cells were found in the AAV-shRAGE group (Fig. 3d). These sortilin-positive cells may play an important role in the progression of calcification. Pearson correlation analysis (Fig. 3e) also revealed that serum sortilin was positive correlated with the maximum of calcium nodule diameters ($r=0.843$, $p<0.05$). Serum sortilin of each group was shown in Table 1. From immunostaining, other cell-derived sortilin-positive cells (such as macrophages) were also found in plaques. However, our present findings do not confirm the close relationship between these sortilin-positive cells and calcification types.

RAGE and galectin-3 regulate calcification patterns of VSMCs

To further investigate the mechanism of calcification patterns, we isolated primary cells from mouse aortic smooth muscles (Supplementary Fig. S4) and established an in vitro model of diabetic vascular calcification. Alizarin red staining was performed after 7 days of culture (Supplementary Fig. S5a, b). We found that after adding oxLDL and 10 μmol/L CML, calcification increased most significantly. Then, VSMCs were cultured with OM, oxLDL and 10 μmol/L CML for 7 or 14 days. Western blotting (Supplementary Fig. S5c) shows that the expression of Runt-Related Transcription Factor 2 (RUNX2) was significantly higher on the 7th day, whereas its expression decreased on the 14th day, which may be related to the cytotoxic effects of CML. So, cells were induced with OM, oxLDL and 10 μmol/L CML for 7 days to establish the in vitro model of diabetic calcification. We chose lentiviral vectors that have reliable transfection efficiency for primary cells. CCK-8 assay (Supplementary Fig. S6) shows that lentivirus transduction did not influence cell viability. From immunofluorescence (Fig. 4a; Supplementary Fig. S7) and RT-PCR (Fig. 4b, c), it can be seen that the level of RAGE was significantly decreased in the LV-shRAGE group, whilst galectin-3 was significantly reduced in the LV-shgalectin-3 group. The blank vector (mock group) had no significant effect on the expression of RAGE or galectin-3. Meanwhile, the calcification morphology (Fig. 4d, f) of the mock group was similar to that of the CML group (64.26 ± 38.91 vs. 58.72 ± 20.07 μm ns.), indicating that the blank vector had no effect on the formation of calcified nodules. The LV-shRAGE group tended to form macrocalcifications (158.15 ± 51.96 μm), while the LV-shgalectin-3 group tended to form microcalcifications (14.17 ± 9.37 μm). The CML, mock, LV-shRAGE, and LV-shgalectin-3 groups had

Table 1 Calcium nodule size and serum sortilin after CML and AAV treatment

	CML	AAV-shscramble	AAV-shRAGE	AAV-shgalectin-3
Major nodule size (μm)	84.01 ± 33.55	86.31 ± 28.61	253.6 ± 99.54	20.77 ± 14.65
Serum sortilin (ng/ml)	30.49 ± 8.17	35.88 ± 13.43	61.2 ± 19.02	13.37 ± 8.55

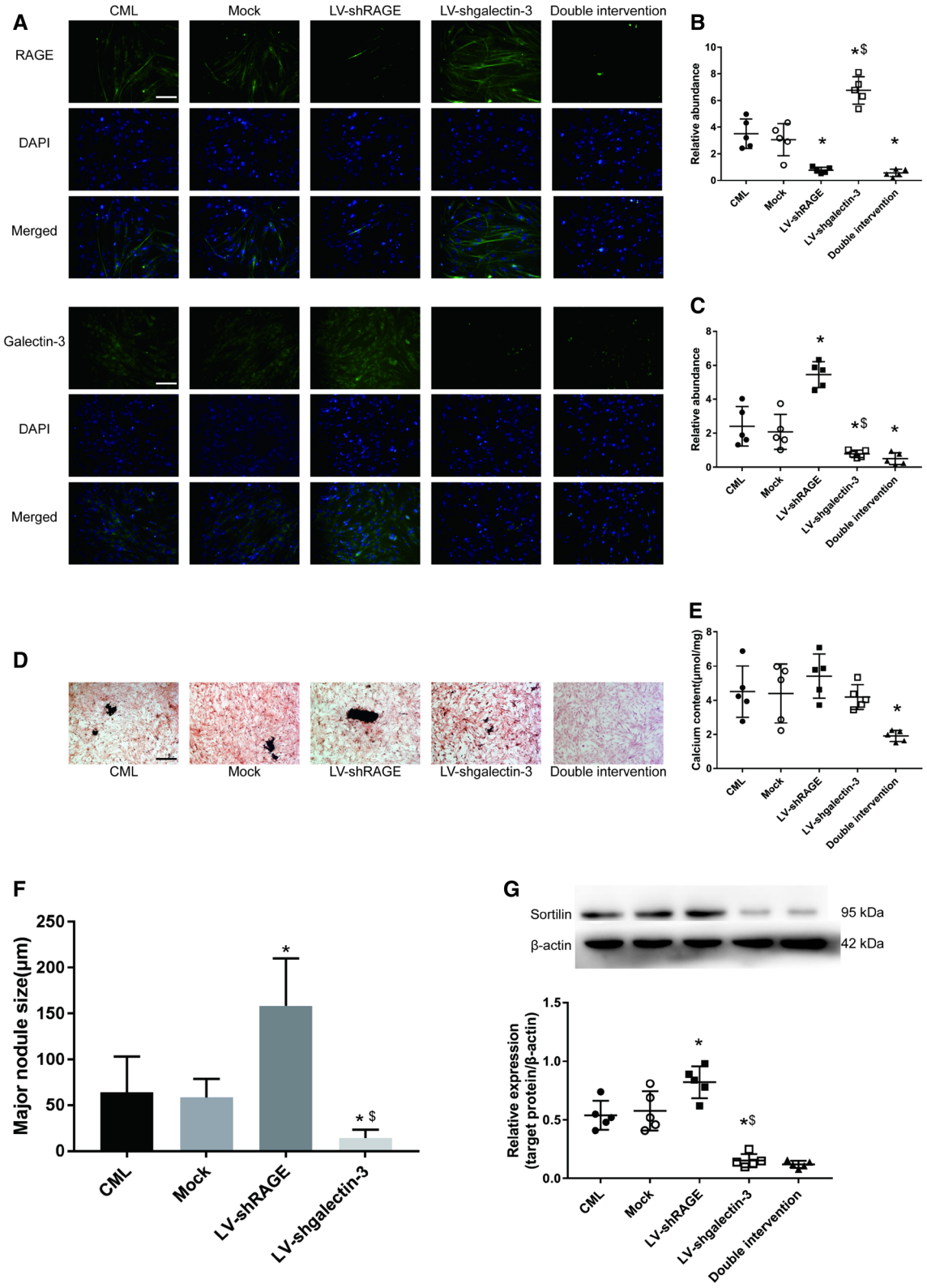

no significant difference in calcium content (Fig. 4e). When RAGE and galectin-3 were both silenced, the calcium content was reduced significantly. Western blotting (Fig. 4g) shows that the expression of sortilin significantly increased in the LV-shRAGE group and noticeably decreased in the LV-shgalectin-3 group. So, it can be inferred that galectin-3 upregulated sortilin, whereas RAGE inhibited sortilin expression.

◂**Fig. 4** RAGE and galectin-3 deliver different signals in the progression of calcification formation in the in vitro diabetic vascular calcification model. **a** Representative images of immunofluorescence staining on the 7th day after LV transfection ($n=5$ independent experienments). Scale 100 μm. **b, c** RAGE and galectin-3 mRNA levels ($n=5$ independent experienments). $^{*}p<0.05$, compared with mock group. $^{\$}p<0.05$, compared with LV-shRAGE group. **d** Von Kossa staining shows calcification morphology under different treatments. Representative images are shown with a scale of 100 μm ($n=5$ independent experienments). LV-shRAGE group had macrocalcification and LV-shgalectin-3 group had microcalcification. Black: calcium deposition. **e** Calcium content of each group ($n=5$ independent experienments). **f** Mean diameter of calcium nodules in each group. **g** Western blot and semi-quantitative analysis show sortilin expression of vascular smooth muscle cells ($n=5$ independent experienments). $^{*}p<0.05$ compared with Mock group; $^{\$}p<0.05$ compared with LV-shRAGE group. (Color figure online)

RAGE/galectin-3 regulated sortilin to further mediate calcification morphology of VSMCs

There were no significant changes in sortilin expression after adding recombinant protein, while sortilin siRNA significantly downregulated sortilin expression (Fig. 5d, e). And, siRNA had no significant effect on cell viability (Supplementary Fig. S6). Von Kossa staining, calcium nodule size and calcium content analysis (Fig. 5a–c) show that the LV-RAGE + scramble and LV-galectin-3 + scramble groups had no significant difference compared with the LV-shRAGE or LV-galectin-3 groups in calcification morphology and quantification. Calcium nodule size and calcium content were clearly increased after adding sortilin recombinant protein. Meanwhile, the calcified nodule size and calcium content were also reduced after blocking sortilin with siRNA. The calcium content reduction of the LV-shRAGE + siRNA group was greater than that of the LV-shgalectin-3 + siRNA group. Compared with the LV-RAGE + scramble group, the calcium content of the LV-RAGE + siRNA group decreased significantly (2.64 ± 0.73 vs. 4.24 ± 1.06 mol/mg, $p<0.05$). Compared with the LV-galectin-3 + scramble group, the calcium content of the LV-galectin-3 + siRNA group was not significantly reduced (3.72 ± 0.45 vs. 4.10 ± 0.93 mol/mg, ns). After 4 days of calcification induction, the samples were examined by SEM (Fig. 5f), which showed that the MVs aggregates of the LV-shRAGE group were larger than those of the LV-galectin-3 group. The aggregates' volume was further increased after treatment with recombinant sortilin protein, and sortilin siRNA partially reversed this progression. NTA (Fig. 5g, h) also shows that the vesicle aggregates diameter of the LV-shRAGE group was significantly increased on the fourth day of calcification induction, which was greater than that of the LV-galectin-3 group (160.22 ± 11.25 vs. 130.59 ± 9.42 μm, $p<0.05$). The diameter further increased with the addition of recombinant sortilin protein and reached 221.77 ± 13.60 μm on the 7th day. We also found that although there was no significant difference in the calcification morphology between the LV-shRAGE + siRNA group and LV-shgalectin-3 + sortilin group, there were differences in the vesicle aggregation patterns between the two groups. Compared with the 1st day, the diameter of vesicles in LV-shRAGE + siRNA group did not change significantly on the 4th day (134.46 ± 8.03 vs. 121.68 ± 11.68 μm, ns). While in LV-shgalectin-3 + sortilin group, the diameter had a significant increase (122.26 ± 10.52 vs. 155.82 ± 7.33 μm, $p<0.05$) on the 4th day. So sortilin may accelerate the accumulation of MVs, leading to the earlier appearance of vesicle aggregates.

Sortilin accelerates matrix vesicle aggregation and affects the calcification process

From in vitro experiments, we initially concluded that RAGE/galectin-3 mediates the calcification outcomes of smooth muscle cells by sortilin. So, a further in vivo study was needed. From von Kossa staining (Fig. 6a), calcium content (Fig. 6b) and calcium nodule analysis (Fig. 6c), we found that compared with the AAV-shRAGE or AAV-shgalectin-3 groups, the AAV-shRAGE + sortilin or AAV-shgalectin-3 + sortilin groups had larger calcium nodule sizes (349.79 ± 74.14 vs. 231.18 ± 78.19 μm, $p<0.05$; 92.38 ± 30.74 vs. 24.19 ± 10.77 μm, $p<0.05$) and more calcium content. After the injection of sortilin antibody, vascular calcification morphology was obviously smaller. SEM (Fig. 6d) shows that at the 3rd week, the AAV-shRAGE + sortilin group had larger MVs aggregates than the AAV-shRAGE group. And, there were no vesicle aggregates in other groups except for the AAV-shRAGE + sortilin group at the 2nd week (results not shown). Although the AAV-shRAGE + anti-sortilin group and AAV-shgalectin-3 + sortilin group had no significant differences in calcification morphology, vesicle aggregation was found in the AAV-shgalectin-3 + sortilin group instead of the AAV-shRAGE + anti-sortilin group at the 3rd week, which also indicated that sortilin could accelerate the formation of MVs aggregates.

Discussion

Previous studies have usually focused on the process of promoting or inhibiting vascular calcification [20, 21]. When we analyzed the calcification conditions of anterior tibial arteries in patients, we found that microcalcifications and macrocalcifications commonly exist in diabetic patients. We constructed a diabetic vascular calcification in vivo mouse model and an in vitro model using mouse-derived VSMCs to

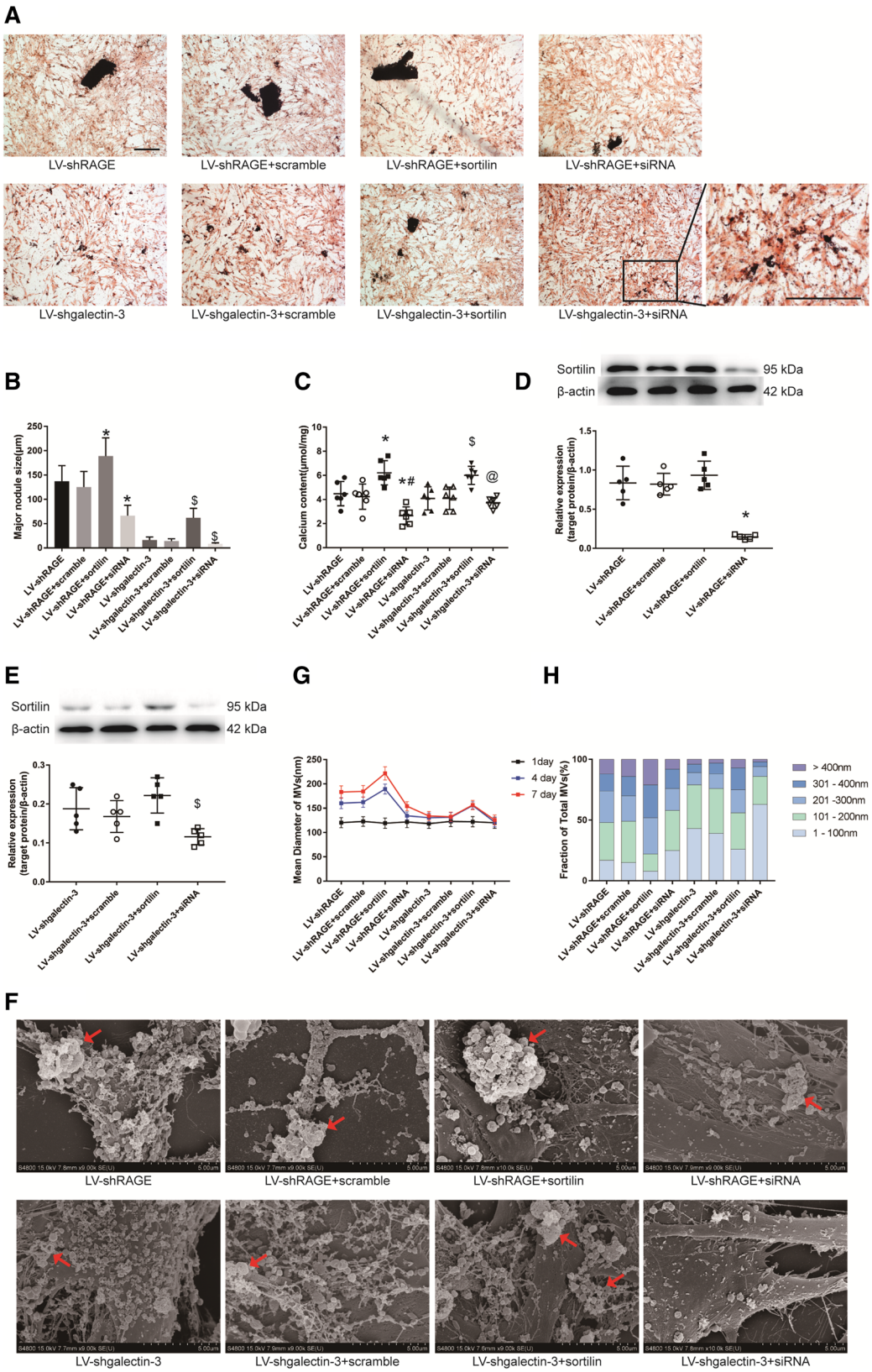
A
LV-shRAGE
LV-shRAGE+scramble
LV-shRAGE+sortilin
LV-shRAGE+siRNA
LV-shgalectin-3
LV-shgalectin-3+scramble
LV-shgalectin-3+sortilin
LV-shgalectin-3+siRNA
B
Major nodule size(μm)
C
Calcium content(μmol/mg)
D
Sortilin
β-actin
95 kDa
42 kDa
Relative expression (target protein/β-actin)
E
Sortilin
β-actin
95 kDa
42 kDa
Relative expression (target protein/β-actin)
G
Mean Diameter of MVs(nm)
1day
4 day
7 day
H
Fraction of Total MVs(%)
> 400nm
301 - 400nm
201 -300nm
101 - 200nm
1 - 100nm
F
LV-shRAGE
LV-shRAGE+scramble
LV-shRAGE+sortilin
LV-shRAGE+siRNA
LV-shgalectin-3
LV-shgalectin-3+scramble
LV-shgalectin-3+sortilin
LV-shgalectin-3+siRNA

◂**Fig. 5** RAGE/galectin-3 leads to changes in sortilin expression and subsequent morphological differences in calcification in the in vitro diabetic vascular calcification model. **a** Representative images of von Kossa staining show the calcified nodules ($n=5$). The calcification morphology was further enlarged when recombinant sortilin protein was added, while the calcification nodules were significantly smaller after sortilin siRNA addition. Black: calcium nodules. Scale bar 100 μm. **b** Mean diameter of major calcium nodules. **c** Calcium content in each group ($n=6$ independent experienments). Sortilin promoted calcification. Blocking of sortilin with siRNA reduced calcification, but its effect on the LV-galectin-3 group was not significant. **d, e** Western blotting and semi-quantitative analysis of sortilin expression ($n=5$ independent experienments). $^{*}p<0.05$ compared with LV-shRAGE + scramble group. $^{\#}p<0.05$ compared with LV-shRAGE + sortilin group. $^{\$}p<0.05$ compared with LV-shgalectin-3 + scramble group. $^{@}p<0.05$ compared with LV-shgalectin-3 + sortilin group. **f** 4 days after calcification induction, SEM revealed that the volume of MVs aggregates was larger in the sortilin addition group. The scale bars are shown at the bottom of each image. **g, h** NTA indicated vesicle aggregate diameters of each group. **g** At 1, 4 and 7 days, diameters of MVs increased in each group and sortilin promoted this process. **h** NTA shows the percentage of MVs in different diameter intervals on the 7th day. (Color figure online)

further investigate the underlying mechanisms. We revealed that RAGE and galectin-3 play different roles in the regulation of calcification morphology. RAGE promoted microcalcification, whereas galectin-3 mediated the formation of macrocalcification. But, the effect of RAGE or galectin-3 on calcium content was not much different. **At the same time, we explored the signaling molecules downstream of RAGE and galectin-3 and found that sortilin acted as the key molecular switch of calcification patterns; targeting of sortilin may have potential clinical application in the future.

In addition, we performed scanning electron microscopy and found that there were differences in the aggregation degree of the MVs (50–500 nm). Such differences may lead to changes in the development of calcification patterns. It has been pointed out that MVs promote mineralization in bone and cartilage tissues [22]. In terms of vascular calcification, osteogenic differentiated smooth muscle cells secret MVs into the extracellular matrix. Then, acicular hydroxyapatite crystals begin to accumulate in vesicles. When the accumulation reaches a certain level, they can pierce the vesicle membrane and spread into the surrounding matrix, which form calcification nodules and islands [23]. The release and aggregation of MVs in the early calcified stage will largely determine the amount and shape of calcified nodules, for calcification slowly expands along the existing calcification baseline [24]. MVs aggregates provide conditions for the formation of larger calcium islands. Larger calcium islands are highly likely to form macrocalcifications.

Sortilin was first discovered in yeast [25], and has since been found to be closely related to many human diseases such as hyperlipidemia [26], diabetes [27], tumorigenesis [28], atherosclerosis [29], B-cell lymphoma [30], and nervous system diseases [31]. Recent studies have also reported that sortilin can transport tissue nonspecific alkaline phosphatase (TNAP) to extracellular vesicles (EVs) during calcification progression, which plays an important role in calcification [32]. TNAP has been confirmed to promote osteogenic differentiation [33]. Vesicles containing TNAP can be endocytosed by surrounding smooth muscle cells [34], which further promotes their trans-differentiation into osteogenic phenotype. And, smooth muscle cells that undergo osteogenic trans-differentiation tend to form macrocalcifications [35]. That is consistent with the results of our study. When suppressing galectin-3, the expression of sortilin decreased, but the calcium content was only slightly reduced indicating that there could be other pro-calcification signals (such as the CML/RAGE calcification cascade) being activated in this process [11]. MVs are a specific subtype of EVs [36], so it can be speculated that sortilin also affects the osteogenic medium in MVs. Whether MVs aggregation is associated with calcification morphology requires further study.

RAGE and galectin-3 are two major receptors for CML, but they seem to have opposite functions. Galectin-3 can eliminate AGEs [37] and play a protective role. Our previous study [10] confirmed that AGEs can promote calcification. In the present study when RAGE was silenced, sortilin increased. However, the increase of calcium content was not substantial, probably due to the removal of AGEs by the upregulated galectin-3. Galectin-3 can also act as an independent mortality predictor of heart failure [38]. Current studies have confirmed that the continuous expression of galectin-3 in the myocardium can induce myocardial remodeling and myocardial fibrosis [39]. In addition, the decrease of vascular compliance induced by macrocalcification is also a potential reason for heart failure.

Conclusion

In summary, the results of our study show that RAGE and galectin-3 play different roles in the regulation of calcification patterns through sortilin (Fig. 7). RAGE inhibited the expression of sortilin and mediated the formation of microcalcification, while galectin-3 promoted the expression of sortilin and induced macrocalcification. In the progression of macrocalcification formation, sortilin accelerated the aggregation of MVs. While MVs aggregation was significantly decelerated in microcalcification, due to the downregulation of sortilin. These findings could provide a worthwhile intervention target for the treatment and prevention of vascular calcification in diabetes, and provide a reference value in clinical risk prediction.

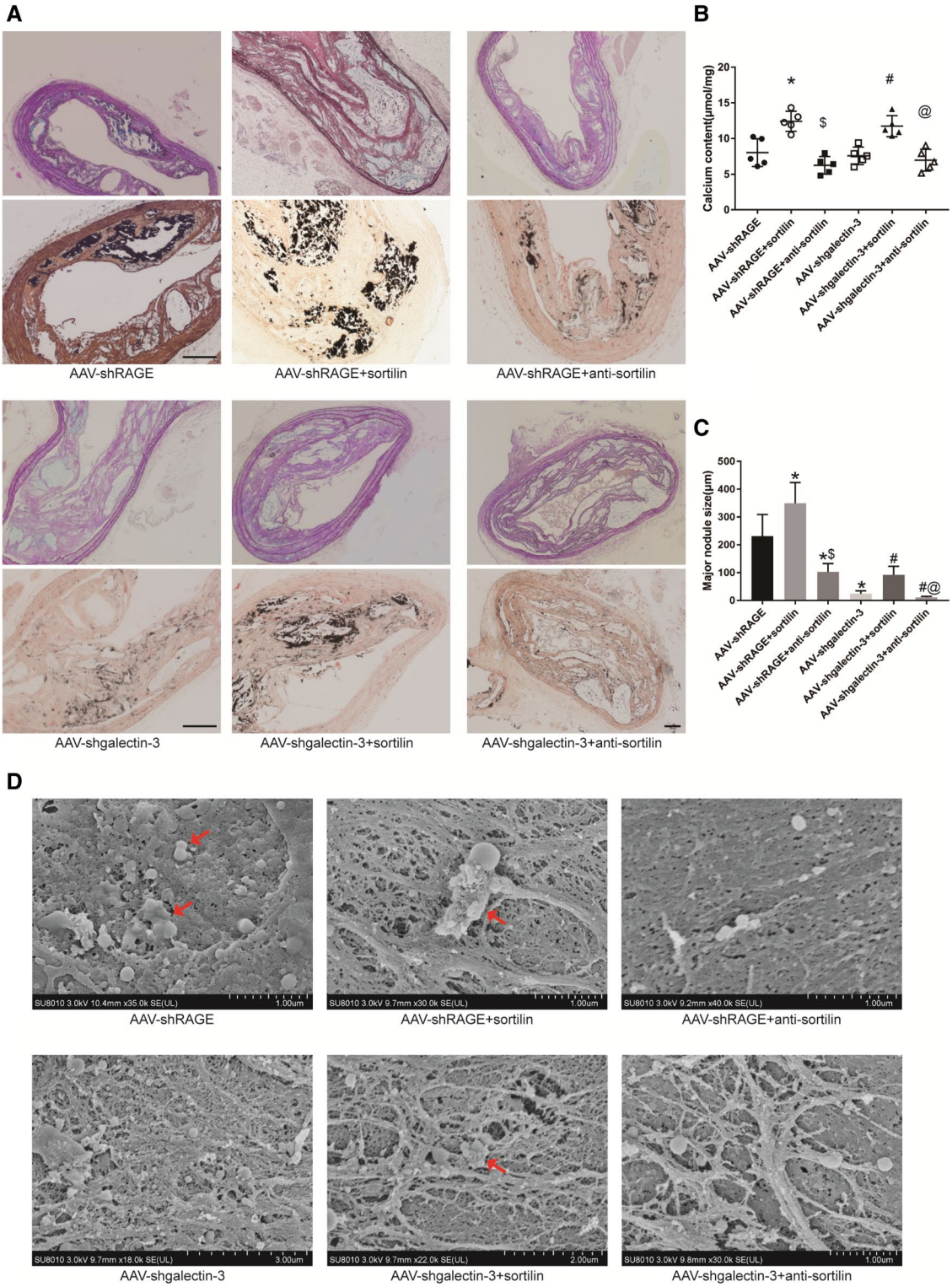

Fig. 6 Effects of RAGE/galectin-3 on aortic calcification with sortilin-related treatment in the diabetic atherosclerosis mouse model. **a** Morphology of vascular calcification as visualized by von Kossa staining after injection of recombinant sortilin protein or sortilin-neutralizing antibody. Serial sections of the aorta were created and representative images of their calcified areas are shown ($n=5$ mice in each group). Black: calcium nodules. Scale 100 μm. **b** Vascular calcium content under different treatments is shown. **c** Mean diameter of major calcium nodules in each group. $^{*}p<0.05$ compared with AAV-shRAGE group. $^{\$}p<0.05$ compared with AAV-shRAGE + sortilin group. $^{\#}p<0.05$ compared with AAV-shgalectin-3 group. $^{@}p<0.05$ compared with AAV-shgalectin-3 + sortilin group. **d** 3 weeks after HFD, SEM of vascular smooth muscles was performed. Red arrows: MVs aggregates. (Color figure online)

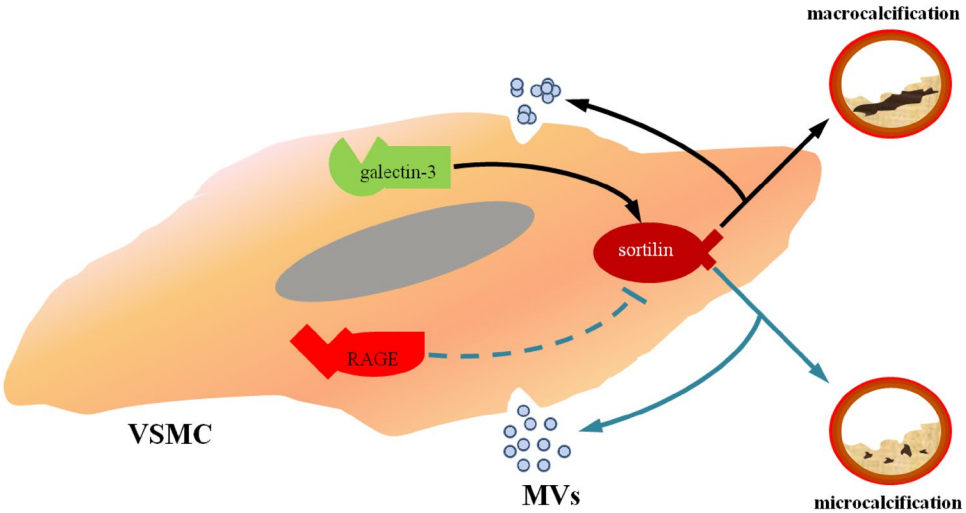

Fig. 7 RAGE inhibits sortilin expression in vascular smooth muscle cells, then forms microcalcification within the plaques. Galectin-3 promotes the expression of sortilin and induces the formation of macrocalcification. And, sortilin can mediate the aggregation of MVs in the early stages of calcification

Author contributions ZS performed, and analyzed experiments, produced figures, and wrote the manuscript. LL contributed to section preparation and immunofluorescence analysis. JY helped the in vivo and in vitro models establishment. CS contributed to gene silencing of cells and mice. ZB helped with SEM and data analysis. LJ contributed to MVs isolation and NTA. YG helped with clinical data collection and analysis. PQ and LZ provided suggestions for experimental design. ZW designed and supervised experiments and wrote the manuscript. All authors read and approved the final manuscript.

Funding This work was supported by the foundations as follows: the National Natural Science Foundation of China (Grant Nos. 81770450, 81370408, 81670405), the Foundation of Jiangsu Province (WSN-044, QNRC2016836), the Open Program of Key Laboratory of Nuclear Medicine, Ministry of Health and Jiangsu Key Laboratory of Molecular Nuclear Medicine (KF201504) and Graduate Student Scientific Research Innovation Projects of Jiangsu Province (KYCX17_1801, SJCX18_0754).

Data availability All data and materials are available upon request.

Compliance with ethical standards

Conflict of interest The authors declare that they have no conflict of interest.

Human and animal rights disclosure Human studies conform to the principles outlined in the Declaration of Helsinki (1964) and was approved by the Ethical Committee of the Affiliated Hospital of Jiangsu University. All animal experiments were approved by the Animal Health and Utilization Committee of the Affiliated Hospital of Jiangsu University, and carried out in accordance with the guidelines from Directive 2010/63/EU and "Principles of laboratory animal care" (NIH publication No. 86-23, revised 1985).

Informed consent All patients gave consent prior to inclusion.

References

1. Benjamin EJ, Virani SS, Callaway CW et al (2018) Heart disease and stroke statistics-2018 update: a report from the american heart association. Circulation 137(12):CIR.0000000000000558
2. Xu S, Ye F, Li L et al (2017) Ghrelin attenuates vascular calcification in diabetic patients with amputation. Biomed Pharmacother 91:1053–1064
3. Singh DK, Winocour P, Summerhayes B et al (2012) Prevalence and progression of peripheral vascular calcification in type 2 diabetes subjects with preserved kidney function. Diabetes Res Clin Pract 97:158–165
4. Kelly-Arnold A, Maldonado N, Laudier D, Aikawa E, Cardoso L, Weinbaum S (2013) Revised microcalcification hypothesis for fibrous cap rupture in human coronary arteries. Proc Natl Acad Sci USA 110:10741–10746
5. Hutcheson JD, Goettsch C, Bertazzo S et al (2016) Genesis and growth of extracellular-vesicle-derived microcalcification in atherosclerotic plaques. Nat Mater 15:335–343
6. Janssen R (2017) Magnesium to counteract elastin degradation and vascular calcification in chronic obstructive pulmonary disease. Med Hypotheses 107:74–77
7. Nakahara T, Dweck MR, Narula N, Pisapia D, Narula J, Strauss HW (2017) Coronary artery calcification: from mechanism to molecular imaging. JACC Cardiovasc Imaging 10:582–593
8. Yao Y, Bennett BJ, Wang X et al (2010) Inhibition of bone morphogenetic proteins protects against atherosclerosis and vascular calcification. Circ Res 107(4):485–494
9. Menini S, Iacobini C, Ricci C et al (2013) The galectin-3/RAGE dyad modulates vascular osteogenesis in atherosclerosis. Cardiovasc Res 100(3):472–480
10. Wang Z, Jiang Y, Liu N et al (2012) Advanced glycation end-product *Nε*-carboxymethyl-Lysine accelerates progression of atherosclerotic calcification in diabetes. Atherosclerosis 221:387–396
11. Wang Z, Li L, Du R et al (2016) CML/RAGE signal induces calcification cascade in diabetes. Diabetol Metab Syndr 8:83–94
12. Zhou Z, Immel D, Xi CX et al (2006) Regulation of osteoclast function and bone mass by RAGE. J Exp Med 203:1067–1080
13. Stock M, Schäfer H, Stricker S, Gross G, Mundlos S, Otto F (2003) Expression of galectin-3 in skeletal tissues is controlled by Runx2. J Biol Chem 278:17360–17367
14. Strong A, Ding Q, Edmondson AC et al (2012) Hepatic sortilin regulates both apolipoprotein B secretion and LDL catabolism. J Clin Invest 122:2807–2816
15. Greenwood SG, Montroull L, Volosin M et al (2018) A novel neuroprotective mechanism for lithium that prevents association of the p75(NTR)-sortilin receptor complex and attenuates proNGF-Induced neuronal death in vitro and in vivo. eNeuro 5:ENEURO.0257-17

16. O'Donnell CJ, Kavousi M, Smith AV et al (2011) Genome-wide association study for coronary artery calcification with follow-up in myocardial infarction. Circulation 124:2855–2864
17. Kaddai V, Jager J, Gonzalez T et al (2009) Involvement of TNF-alpha in abnormal adipocyte and muscle sortilin expression in obese mice and humans. Diabetologia 52:932–940
18. Kjolby M, Andersen OM, Breiderhoff T et al (2010) Sort1, encoded by the cardiovascular risk locus 1p13.3, is a regulator of hepatic lipoprotein export. Cell Metab 12:213–223
19. Alves RD, Eijken M, Bezstarosti K, Demmers JA, van Leeuwen JP (2013) Activin A suppresses osteoblast mineralization capacity by altering extracellular matrix (ECM) composition and impairing matrix vesicle (MV) production. Mol Cell Proteomics 12:2890–2900
20. Gungor O, Kocyigit I, Yilmaz MI, Sezer S (2018) Role of vascular calcification inhibitors in preventing vascular dysfunction and mortality in hemodialysis patients. Semin Dial 31:72–81
21. Pérez-Hernández N, Aptilon-Duque G, Blachman-Braun R et al (2017) Vascular calcification: current genetics underlying this complex phenomenon. Chin Med J (Engl) 130:1113–1121
22. Cui L, Houston DA, Farquharson C, MacRae VE (2016) Characterisation of matrix vesicles in skeletal and soft tissue mineralisation. Bone 87:147–158
23. Zazzeroni L, Faggioli G, Pasquinelli G (2018) Mechanisms of arterial calcification: the role of matrix vesicles. Eur J Vasc Endovasc Surg 55:425–433
24. Moe SM, O'Neill KD, Duan D et al (2002) Medial artery calcification in ESRD patients is associated with deposition of bone matrix proteins. Kidney Int 61:638–647
25. Marcusson EG, Horazdovsky BF, Cereghino JL, Gharakhanian E, Emr SD (1994) The sorting receptor for yeast vacuolar carboxypeptidase Y is encoded by the VPS10 gene. Cell 77:579–586
26. Linsel-Nitschke P, Heeren J, Aherrahrou Z et al (2010) Genetic variation at chromosome 1p13.3 affects sortilin mRNA expression, cellular LDL-uptake and serum LDL levels which translates to the risk of coronary artery disease. Atherosclerosis 208:183–189
27. Bi L, Chiang JY, Ding WX, Dunn W, Roberts B, Li T (2013) Saturated fatty acids activate ERK signaling to downregulate hepatic sortilin 1 in obese and diabetic mice. J Lipid Res 54:2754–2762
28. Béraud-Dufour S, Devader C, Massa F, Roulot M, Coppola T, Mazella J (2016) Focal adhesion kinase-dependent role of the soluble form of neurotensin receptor-3/sortilin in colorectal cancer cell dissociation. Int J Mol Sci 17:1860
29. Patel KM, Strong A, Tohyama J et al (2015) Macrophage sortilin promotes LDL uptake, foam cell formation, and atherosclerosis. Circ Res 116:789–796
30. Saada S, Marget P, Fauchais AL et al (2012) Differential expression of neurotensin and specific receptors, NTSR1 and NTSR2, in normal and malignant human B lymphocytes. J Immunol 189:5293–5303
31. Gustafsen C, Glerup S, Pallesen LT et al (2013) Sortilin and SorLA display distinct roles in processing and trafficking of amyloid precursor protein. J Neurosci 33:64–71
32. Goettsch C, Hutcheson JD, Aikawa M et al (2016) Sortilin mediates vascular calcification via its recruitment into extracellular vesicles. J Clin Invest 126:1323–1336
33. Patel JJ, Zhu D, Opdebeeck B et al (2018) Inhibition of arterial medial calcification and bone mineralization by extracellular nucleotides: The same functional effect mediated by different cellular mechanisms. J Cell Physiol 233:3230–3243
34. Chen NX, O'Neill KD, Moe SM (2018) Matrix vesicles induce calcification of recipient vascular smooth muscle cells through multiple signaling pathways. Kidney Int 93:343–354
35. Shioi A, Ikari Y (2017) Plaque calcification during atherosclerosis progression and regression. J Atheroscler Thromb 25:294–303
36. Bakhshian Nik A, Hutcheson JD, Aikawa E (2017) Extracellular vesicles as mediators of cardiovascular calcification. Front Cardiovasc Med 4:78
37. Pugliese G, Iacobini C, Pesce CM, Menini S (2015) Galectin-3: an emerging all-out player in metabolic disorders and their complications. Glycobiology 25:136–150
38. Savic-Radojevic A, Pljesa-Ercegovac M, Matic M, Simic D, Radovanovic S, Simic T (2017) Novel biomarkers of heart failure. Adv Clin Chem 79:93–152
39. Suthahar N, Meijers WC, Silljé HHW, Ho JE, Liu FT, de Boer RA (2018) Galectin-3 activation and inhibition in heart failure and cardiovascular disease: an update. Theranostics 8:593–609

Affiliations

Zhen Sun[1] · Zhongqun Wang[1] · Lihua Li[2] · Jinchuan Yan[1] · Chen Shao[1] · Zhengyang Bao[1] · Lele Jing[1] · Qiwen Pang[1] · Yue Geng[1] · Lili Zhang[1]

Zhen Sun
sunfy893@foxmail.com

Lihua Li
tsmc01@163.com

Jinchuan Yan
yanjinchuan@hotmail.com

Chen Shao
shaochen84@163.com

Zhengyang Bao
490213060@qq.com

Lele Jing
459736150@qq.com

Qiwen Pang
352719816@qq.com

Yue Geng
1179536890@qq.com

Lili Zhang
2893196597@qq.com

[1] Department of Cardiology, Affiliated Hospital of Jiangsu University, 212001 Zhenjiang, China

[2] Department of Pathology, Affiliated Hospital of Jiangsu University, 212001 Zhenjiang, China